Synthetic Aperture Radar Imaging of Moving Targets Using Ultra-Narrowband Continuous Waveforms

Ling Wang
College of Electronic and Information Engineering, Nanjing University of Aeronautics and Astronautics, Nanjing 210016, China

Birsen Yazıcı
Department of Electrical, Computer and Systems Engineering, Rensselaer Polytechnic Institute, 110 8th Street, Troy, NY 12180 USA E-mail: yazici@ecse.rpi.edu

Abstract

We present a novel method of imaging multiple moving targets using a SAR system transmitting ultra-narrowband continuous waveforms. Our method comprises of a new forward model that relates the velocity as well as reflectivity information at each location to a correlated received signal; and a novel image formation method based on filtered-backprojection and image-contrast optimization. The method results in well-focused reflectivity images of moving targets and their velocity estimates regardless of the target location, speed, and velocity direction. We present numerical experiments to demonstrate the performance of our imaging method.

1 Introduction

Traditional synthetic aperture radar (SAR) systems accomplish high-range resolution imaging of static scenes and moving targets by transmitting wideband waveforms [1–6]. In this paper, we consider a SAR system that transmits ultra-narrowband continuous waveforms. This system requires a relatively simple and low-cost transmitter, and in some cases does not need a dedicated transmitter. Existing radio frequency signals, such as radio, television signals, etc. can be used as the transmission sources. Additionally, ultra-narrowband continuous waveforms have high Doppler resolution and are capable of capturing the velocity information of the moving targets as compared to the high range resolution waveforms used by the traditional SAR systems.

In [7], we presented a novel method of imaging stationary scenes that takes advantage of the high Doppler resolution of the transmitted ultra-narrowband continuous waveforms. In this paper, we consider the moving target imaging problem using such SAR systems. Our approach exploits the high Doppler resolution of the transmitted waveforms to reconstruct the reflectivity (position), as well as to estimate the velocity field of moving targets. We develop a novel model that relates the velocity field and the reflectivity of the scene to a correlated received signal; and a corresponding FBP-type novel image formation and an image-contrast optimization method to determine the reflectivity and velocity field of a moving scene. The method is capable of localizing and estimating the velocity of targets with high resolution regardless of the target location, speed and velocity direction.

The organization of the paper is as follows: In Section 2, we present the model for the received signal scattered from a scene with multiple moving targets and develop the forward model for imaging of moving targets. In Section 3, we develop an FBP-type image formation method and a velocity estimation method. In Section 4, we present numerical simulations to verify our imaging method for moving targets. Section 5 concludes our paper.

2 Forward Model for Imaging

2.1 Received Signal Model for Multiple Moving Targets

Let $\mathbf{z} = (\boldsymbol{z}, \psi(\boldsymbol{z})) \in \mathbb{R}^3$ denote the earth's surface, where $\boldsymbol{z} \in \mathbb{R}^2$ and $\psi : \mathbb{R}^2 \to \mathbb{R}$ is a known function for the ground topography. Let $\mathbf{\Gamma}(\mathbf{z}, t)$ denote the trajectory of the target located at $\mathbf{z}$ when $t = 0$. We assume that $\mathbf{\Gamma}(\mathbf{z}, t)$ has the form $\mathbf{\Gamma}(\mathbf{z}, t) = \mathbf{z} + \mathbf{\Gamma}_{\mathbf{z}}(t)$ where $\mathbf{\Gamma}_{\mathbf{z}}(t)$, $\mathbf{z} = [\boldsymbol{z}, \psi(\boldsymbol{z})]$, $\boldsymbol{z} \in \mathbb{R}^2$, is a family of one-parameter curves in three dimensional space that describe the trajectories of the targets. Thus, for the ground moving targets, $\mathbf{\Gamma}^3_{\mathbf{z}}(t) = \psi([\mathbf{\Gamma}^1_{\mathbf{z}}(t), \mathbf{\Gamma}^2_{\mathbf{z}}(t)])$ where $\mathbf{\Gamma}_{\mathbf{z}}(t) = [\mathbf{\Gamma}^1_{\mathbf{z}}(t), \mathbf{\Gamma}^2_{\mathbf{z}}(t), \mathbf{\Gamma}^3_{\mathbf{z}}(t)]$. Note that for stationary targets, $\mathbf{\Gamma}_{\mathbf{z}}(t) = 0$ for all $t \geq 0$.

Let $\mathbf{v}_{\mathbf{z}}$ denote the velocity of the moving scatterer located at $\boldsymbol{z}$ at $t = 0$. Then, $\mathbf{v}_{\mathbf{z}} = \dot{\mathbf{\Gamma}}_{\mathbf{z}}(t) = [\boldsymbol{v}_{\boldsymbol{z}}, D\psi(\boldsymbol{z}) \cdot \boldsymbol{v}_{\boldsymbol{z}}]$ where $\boldsymbol{v}_{\boldsymbol{z}} = [\dot{\mathbf{\Gamma}}^1_{\mathbf{z}}(t), \dot{\mathbf{\Gamma}}^2_{\mathbf{z}}(t)]$ and $D\psi(\boldsymbol{z}) = [\frac{\partial \psi}{\partial z_1} \quad \frac{\partial \psi}{\partial z_2}]$. Note that $\mathbf{v}_{\mathbf{z}}$ may be t dependent. However, we drop t for the notational simplicity.

Let $\rho(\mathbf{z})$ denote the reflectivity function of the scene at time $t = 0$. At time t, taking into account the movement of the scatters, the reflectivity function translates as

$$\begin{aligned}\rho(\mathbf{x} - \mathbf{\Gamma}_{\mathbf{z}}(t)) \simeq\ & \tilde{\rho}(\boldsymbol{x} - \boldsymbol{v}_{\boldsymbol{z}} t)\delta(x_3 - \psi(\boldsymbol{x})) \\ & \times \delta(v_3 - D\psi(\boldsymbol{x}) \cdot \boldsymbol{v}_{\boldsymbol{z}}) \\ =:\ & q_{\boldsymbol{v}_{\boldsymbol{z}}}(\boldsymbol{x}) \end{aligned} \tag{1}$$

where $\mathbf{z} = \mathbf{\Gamma}^{-1}(\mathbf{x}, t)$.

Let $\boldsymbol{\gamma}_T(t)$ and $\boldsymbol{\gamma}_R(t)$ be the transmitter and receiver trajectories, respectively; and $p(t)$ denote the transmitted waveform and $r(t)$ denote the received signal. We consider a finite and relatively short receiving time-window starting at time $t = s$.

Using the scalar wave equation along with (1), under the Born approximation and, taking into account the fact that the velocities of the antennas and targets are much less than the speed of light; and under the assumption that the range variation due to the movement of the antennas and the scene is much less than the the transmitter-to-scene and scene-to-receiver range, we have

$$r(t+s) \approx \int \frac{p(\alpha t - \tau + s) q_{\boldsymbol{v}_{\boldsymbol{z}}}(\boldsymbol{z})}{(4\pi)^2 G_{TR}(s, \boldsymbol{z}, \boldsymbol{v}_{\boldsymbol{z}})} d\boldsymbol{z} d\boldsymbol{v}_{\boldsymbol{z}}\,, \tag{2}$$

where G_{TR} is the product of the geometrical spreading factors given by

$$\begin{aligned} G_{TR}(s, \boldsymbol{z}, \boldsymbol{v}_{\boldsymbol{z}}) =& |\boldsymbol{\gamma}_T(s) - (\mathbf{z} + \mathbf{\Gamma}_{\mathbf{z}}(s))| \\ & \times |\boldsymbol{\gamma}_R(s) - (\mathbf{z} + \mathbf{\Gamma}_{\mathbf{z}}(s))|\,, \end{aligned} \tag{3}$$

the time dilation $\alpha \approx 1 + \beta$ with β given by

$$\begin{aligned} \beta =& [(\boldsymbol{\gamma}_T(s) - \widehat{(\mathbf{z} + \mathbf{\Gamma}_{\mathbf{z}}(s))}) \cdot (\mathbf{v}_{\mathbf{z}} - \dot{\boldsymbol{\gamma}}_T(s)) \\ & + (\boldsymbol{\gamma}_R(s) - \widehat{(\mathbf{z} + \mathbf{\Gamma}_{\mathbf{z}}(s))}) \cdot (\mathbf{v}_{\mathbf{z}} - \dot{\boldsymbol{\gamma}}_R(s))]/c_0\,, \end{aligned} \tag{4}$$

and the time delay τ is approximately given by

$$\tau \approx [|\boldsymbol{\gamma}_T(s) - (\mathbf{z} + \mathbf{\Gamma}_{\mathbf{z}}(s))| + |\boldsymbol{\gamma}_R(s) - (\mathbf{z} + \mathbf{\Gamma}_{\mathbf{z}}(s))|]/c_0\,. \tag{5}$$

Note that $f_0\beta$ ($f_0 = \omega_0/2\pi$) represents the total Doppler frequency induced by the relative radial motion of the antennas and the moving scatters. We refer to it as the *bistatic Doppler frequency for moving targets* and denote it with $f_d(s, \boldsymbol{z}, \boldsymbol{v}_{\boldsymbol{z}})$, i.e.,

$$\begin{aligned} f_d(s, \boldsymbol{z}, \boldsymbol{v}_{\boldsymbol{z}}) =& \frac{f_0}{c_0} [(\boldsymbol{\gamma}_T(s) - \widehat{(\mathbf{z} + \mathbf{\Gamma}_{\mathbf{z}}(s))}) \cdot (\mathbf{v}_{\mathbf{z}} - \dot{\boldsymbol{\gamma}}_T(s)) \\ & + (\boldsymbol{\gamma}_R(s) - \widehat{(\mathbf{z} + \mathbf{\Gamma}_{\mathbf{z}}(s))}) \cdot (\mathbf{v}_{\mathbf{z}} - \dot{\boldsymbol{\gamma}}_R(s))]\,. \end{aligned} \tag{6}$$

In (4) and (6), $\mathbf{v}_{\mathbf{z}} = \dot{\mathbf{\Gamma}}_{\mathbf{z}}(s)$ denotes the velocity of the moving scatter at $t = s$. In the following discussion, we assume that the targets are moving linearly. Thus, $\mathbf{v}_{\mathbf{z}}$ is a time independent quantity.

For a narrowband waveform, we have $p(t) = \mathrm{e}^{\mathrm{i}\omega_0 t}\tilde{p}(t)$ where ω_0 denotes the carrier frequency and $\tilde{p}(t)$ is the complex envelope of p, which is slow varying as a function of t as compared to $\mathrm{e}^{\mathrm{i}\omega_0 t}$. Thus, we have

$$r(t+s) = \int \frac{\tilde{p}(\alpha t - \tau + s)\mathrm{e}^{\mathrm{i}\omega_0(\alpha t - \tau + s)} q_{\boldsymbol{v}_{\boldsymbol{z}}}(\boldsymbol{z})}{(4\pi)^2 G_{TR}(s, \boldsymbol{z}, \boldsymbol{v}_{\boldsymbol{z}})} d\boldsymbol{z} d\boldsymbol{v}_{\boldsymbol{z}} \tag{7}$$

where α and τ are as defined above.

2.2 Forward Model

We define the correlation of the received signal given by (2) with a scaled or frequency-shifted version of the transmitted signal over a finite time window by

$$d(s, \mu) = \int r(t+s) p^*(\mu t)\phi(t) dt \tag{8}$$

for some $s \in \mathbb{R}$ and $\mu \in \mathbb{R}^+$, where $\phi(t)$ is a smooth windowing function starting at $t = 0$ with a finite support. Substituting (7) into (8), we obtain

$$\begin{aligned} d(s, \mu) = \int & \frac{\mathrm{e}^{\mathrm{i}\omega_0(\alpha - \mu)t}\mathrm{e}^{\mathrm{i}\omega_0(s - \tau)}}{(4\pi)^2 G_{TR}(s, \boldsymbol{z}, \boldsymbol{v}_{\boldsymbol{z}})} \\ & \times \tilde{p}(\alpha t - \tau + s)\tilde{p}^*(\mu t) q_{\boldsymbol{v}_{\boldsymbol{z}}}(\boldsymbol{z}) d\boldsymbol{z} d\boldsymbol{v}_{\boldsymbol{z}} dt\,. \end{aligned} \tag{9}$$

The forward model for the bistatic synthetic aperture imaging of moving targets using ultra-narrowband CW signals becomes

$$\begin{aligned} & d(s, \mu) \approx \mathcal{F}[q_{\boldsymbol{v}_{\boldsymbol{z}}}](s, \mu) \\ & = \int \mathrm{e}^{-\mathrm{i}\phi(t, \boldsymbol{z}, \boldsymbol{v}_{\boldsymbol{z}}, s, \mu)} A(t, \boldsymbol{z}, \boldsymbol{v}_{\boldsymbol{z}}, s, \mu) q_{\boldsymbol{v}_{\boldsymbol{z}}}(\boldsymbol{z}) d\boldsymbol{z} d\boldsymbol{v}_{\boldsymbol{z}} dt \end{aligned} \tag{10}$$

where

$$\phi(t, \boldsymbol{z}, \boldsymbol{v}_{\boldsymbol{z}}, s, \mu) = 2\pi f_0 t[(\mu - 1) - f_d(s, \boldsymbol{z}, \boldsymbol{v}_{\boldsymbol{z}})/f_0]\,, \tag{11}$$

$$A(t, \boldsymbol{z}, \boldsymbol{v}_{\boldsymbol{z}}, s, \mu) = \frac{\tilde{p}(\alpha t - \tau + s)\tilde{p}^*(\mu t)\mathrm{e}^{\mathrm{i}\omega_0(s - \tau)}}{(4\pi)^2 G_{TR}(s, \boldsymbol{z}, \boldsymbol{v}_{\boldsymbol{z}})}\,. \tag{12}$$

We refer to $\mathcal{F}$ as the forward modeling operator. We assume that for some m_A, A satisfies the inequality

$$\begin{aligned} \sup_{(t, \mu, s, \boldsymbol{z}, \boldsymbol{v}_{\boldsymbol{z}}) \in \mathcal{U}} & \left|\partial_t^{\alpha_t}\partial_\mu^{\alpha_\mu}\partial_s^{\beta_s}\partial_{z_1}^{\epsilon_1}\partial_{z_2}^{\epsilon_2}\partial_{v_1}^{\varepsilon_1}\partial_{v_2}^{\varepsilon_2} A(t, \boldsymbol{z}, \boldsymbol{v}_{\boldsymbol{z}}, s, \mu)\right| \\ & \leq C_A(1 + t^2)^{(m_A - |\alpha_t|)/2} \end{aligned} \tag{13}$$

where $\mathcal{U}$ is any compact subset of $\mathbb{R} \times \mathbb{R}^+ \times \mathbb{R} \times \mathbb{R}^2 \times \mathbb{R}^2$, and the constant C_A depends on $\mathcal{U}, \alpha_{t,\mu}, \beta_s, \epsilon_{1,2}, \varepsilon_{1,2}$. This assumption is needed in order to make various stationary phase calculations hold.

Under the assumption (13), (10) defines $\mathcal{F}$ as a *Fourier integral operator* whose leading-order contribution comes from those points lying in the four-dimensional space $(\boldsymbol{z}, \boldsymbol{v}_{\boldsymbol{z}})$ having the same bistatic Doppler frequency for moving targets, i.e., $\{(\boldsymbol{z}, \boldsymbol{v}_{\boldsymbol{z}}) \in \mathbb{R}^2 \times \mathbb{R}^2 : f_d(s, \mathbf{z}, \boldsymbol{v}_{\boldsymbol{z}}) = f_0(\mu - 1)\}$. We denote this four-dimensional manifold by

$$F(s, \mu) = \{(\boldsymbol{z}, \boldsymbol{v}_{\boldsymbol{z}}) : f_d(s, \boldsymbol{z}, \boldsymbol{v}_{\boldsymbol{z}}) = f_0(\mu - 1)\} \tag{14}$$

and refer to $F(s, \mu)$ as the bistatic iso-Doppler manifold.

3 Image Formation

Given the data $d(s,\mu)$, we form the image $q_{\boldsymbol{v_z}}(\boldsymbol{z})$ in the $(\boldsymbol{z},\boldsymbol{v_z})$ space by filtering and backprojecting the data onto $F(s,\mu)$, from which we localize the targets at $t=0$ and determine their corresponding velocities as described below.

3.1 FBP Image Formation

We form the image $q_{\boldsymbol{v_z}}(\boldsymbol{z})$ with a hypothesized velocity $\boldsymbol{v}_h$ by the filtered-backprojection method as follows:

$$\begin{aligned}\tilde{q}_{\boldsymbol{v}_h}(\boldsymbol{z}) &:= \mathcal{K}_{\boldsymbol{v}_h}[d]\boldsymbol{z} \\ &= \int \mathrm{e}^{\mathrm{i}\phi(t,\boldsymbol{z},\boldsymbol{v}_h,s,\mu)} Q(\boldsymbol{z},\boldsymbol{v}_h,t,s) d(s,\mu) dt ds d\mu, \end{aligned} \quad (15)$$

where $\mathcal{K}_{\boldsymbol{v}_h}$ is referred to as the filtered-backprojection operator where Q is the underlying filter.

We determine Q so that the point spread function of the resulting imaging operator for $\boldsymbol{v}_h = \boldsymbol{v}_z$ is approximately a Dirac delta function. Similar to the derivation in [7], we obtain

$$Q(\boldsymbol{z},\boldsymbol{v}_h,t,s) = \frac{\chi_{\Omega_{s,\boldsymbol{z},\boldsymbol{v}_h}}}{\eta(s,\boldsymbol{z},\boldsymbol{v}_h,\boldsymbol{\xi})} \frac{A^*(t,\boldsymbol{z},\boldsymbol{v}_h,s)}{|A(t,\boldsymbol{z},\boldsymbol{v}_h,s)|^2} \quad (16)$$

where $A(t,\boldsymbol{z},\boldsymbol{v}_h,s) = A(t,\boldsymbol{z},\boldsymbol{v}_h,s,1+f_d(s,\boldsymbol{z},\boldsymbol{v}_h)/f_0)$, $\chi_{\Omega_{s,\boldsymbol{z},\boldsymbol{v}_h}}$ is a smooth cut-off function equal to one in the interior of $\Omega_{s,\boldsymbol{z},\boldsymbol{v}_h}$ and zero in the exterior of $\Omega_{s,\boldsymbol{z},\boldsymbol{v}_h}$, and $\eta(s,\boldsymbol{z},\boldsymbol{v}_h,\boldsymbol{\xi})$ is the determinant of the Jacobian that comes from the change of variables: $(t,s) \rightarrow \boldsymbol{\xi} = 2\pi t \nabla_{\boldsymbol{z}} f d(s,\boldsymbol{z},\boldsymbol{v}_h)$.

With this choice of filter, the visible edges of the scene can be reconstructed not only at the correct location and orientation, but also at the correct strength when $\boldsymbol{v}_h = \boldsymbol{v_z}$ [8].

3.2 Determination of the Scene Reflectivity and Velocity Field

The filtered-backprojection (FBP) of $d(s,\mu)$ results in a set of reflectivity images $\tilde{q}_{\boldsymbol{v}_h}$ in the two-dimensional $\boldsymbol{z}$ space for each velocity value $\boldsymbol{v_h}$ for a range of velocities that is suitably chosen for ground moving targets. When the hypothesized velocity $v_{\boldsymbol{h}}$ is equal to the correct velocity $v_{\boldsymbol{z}}$, the corresponding reflectivity image is expected to be well-focused. We measure the degree to which the reflectivity images are focused with the image contrast and generate a contrast-image defined as follows:

$$I(v_{h1}, v_{h2}) = \mathcal{C}[\tilde{q}_{\boldsymbol{v}_h}] \quad (17)$$

where $\mathcal{C}$ denotes the contrast operator [9] and $\boldsymbol{v}_h = (v_{h1}, v_{h2})$ is used as the index of the contrast image. We determine the velocity of the moving scatterers by localizing the local maxima in the contrast-image $I(\boldsymbol{v}_h)$.

4 Numerical Simulations

We performed numerical simulations to demonstrate the theoretical results and the performance of the imaging method described in sections 2 and 3.

We considered a scene of size $[0,11]\times[0,11]\,\mathrm{km}^2$ with flat topography centered at $[11,11,0]\mathrm{km}$. The scene was discretized into 128×128 pixels, where $[0,0,0]\mathrm{m}$ and $[11,11,0]\mathrm{km}$ correspond to the pixels $(1,1)$ and $(128,128)$, respectively. Fig. 1 shows the scene with a static extended target and multiple moving targets along with their corresponding velocities. 00

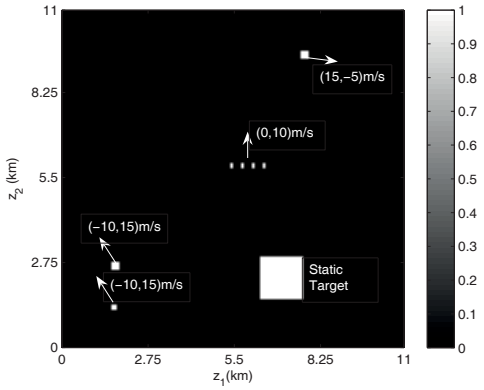

Figure 1: Scene considered in the numerical simulations

We assumed that the transmitter and receiver were traversing a circular trajectory given by $\gamma_C(s) = (11 + 11\cos(s), 11 + 11\sin(s), 6.5)\,\mathrm{km}$. Let $\boldsymbol{\gamma}_T(s)$ and $\boldsymbol{\gamma}_R(s)$ denote the trajectories of the two receivers. We set $\boldsymbol{\gamma}_T(s) = \gamma_C(s)$ and $\boldsymbol{\gamma}_R(s) = \gamma_1(s - \frac{\pi}{4})$. Note that the variable s in γ_C is equal to $\frac{V}{R}t$ where V is the speed of the receiver, and R is the radius of the circular trajectory. We set the speed of the two receivers to $261\,\mathrm{m/s}$.

We assumed that the transmitter transmitted a single-frequency continuous waveform operating at $f_0 = \omega_0/2\pi = 800\mathrm{MHz}$. We used (7) and (8) to generate the data. The length of the signal was set to $0.1707\mathrm{s}$. The circular trajectory was uniformly sampled into 2048 points.

We assumed that the velocity of the targets is in the range of $[-20,20]\times[-20,20]\mathrm{m/s}$ and reconstructed $q_{\boldsymbol{v}_h}(\boldsymbol{z})$ images via the FBP and image-contrast optimization method as described in Section 3. We see from Fig. 2 that there are four dominant peaks marked with red circles in the contrast-image. This indicates that there are four different velocities associated with the targets in the scene. The velocities where the peaks are located are equal to the velocities of the targets we assumed in the simulations.

Fig. 3 presents the reconstructed images using the four estimated velocities. We observe that the targets are well-focused in the image formed using the correct velocity associated with each target.Note that Fig. 3(a) is the image reconstructed with $\mathbf{v}_h = [0,0,0]\mathrm{m/s}$. In this case, the

moving target imaging method described here is equivalent to the static target imaging method in [7]. As expected only the static target is well-focused in Fig. 3(a).

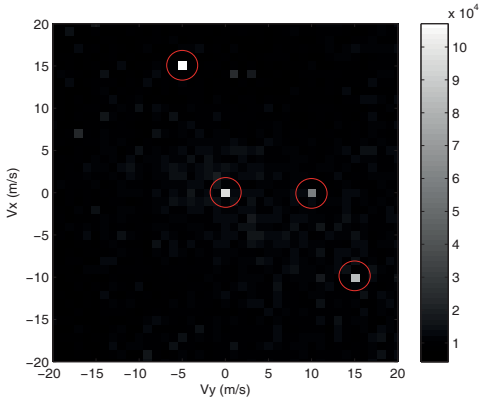

Figure 2: The contrast-image formed by the contrast of the images reconstructed with each hypothesized velocity.

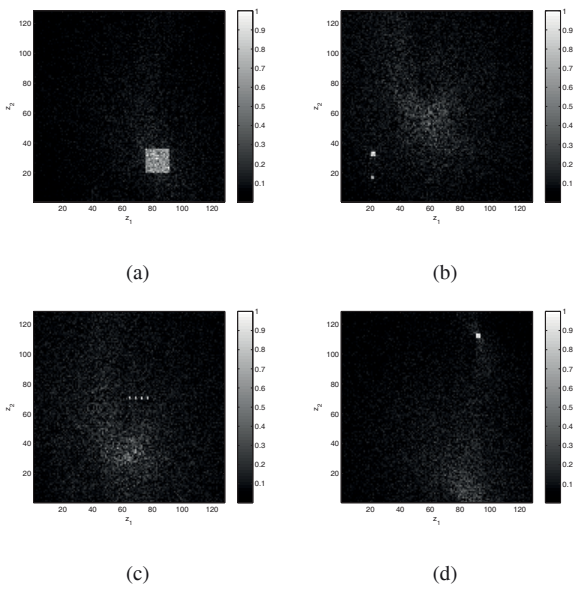

Figure 3: Reconstructed images with the target velocities: (a) $\mathbf{v}_h = [0, 0, 0]\mathrm{m/s}$; (b) $\mathbf{v}_h = [-10, 15, 0]\mathrm{m/s}$; (c) $\mathbf{v}_h = [0, 10, 0]\mathrm{m/s}$; (d) $\mathbf{v}_h = [15, -5, 0]\mathrm{m/s}$.

5 Conclusion

In this paper, we considered the problem of synthetic aperture radar imaging of moving targets using ultra-narrowband transmitted waveforms. We presented a received signal model for a dynamic scene and a novel forward model for image formation. We developed an associated novel FBP and image-contrast optimization based image formation method to estimate the velocities of multiple targets and their corresponding reflectivity images. We presented numerical simulations to verify the theoretical results. A complete analysis of the performance of our imaging method and demonstration of its performance in more realistic scenarios will be the focus of our future work.

Acknowledgement

This work was supported by the Air Force Office of Scientific Research (AFOSR) under the agreements FA9550-07-1-0363 and FA9550-09-1-0013, and by the National Science Foundation (NSF) under Grant No. CCF-08030672.

References

[1] W. C. Carrara, R. G. Goodman, and R. M. Majewski, *Spotlight Synthetic Aperture Radar: Signal Processing Algorithms*, Artech House, Boston, 1995.

[2] J. K. Jao, "Theory of synthetic aperture radar imaging of a moving target," *IEEE Trans. on Geoscience and Remote Sensing*, vol. 39, pp. 1984–1992, September 2001.

[3] M. Kirscht, "Detection and imaging of arbitrarily moving targets with single-channel SAR," *IEE Proc. on Radar Sonar Navig.*, vol. 150, pp. 7–11, February 2003.

[4] M. J. Minardi, L. A. Gorham, and E. G. Zelnio, "Ground moving target detection and tracking based on generalized SAR processing and change detection," in *Proc. of SPIE on Defense, Security and Sensing, Bellingham, WA, USA*, April 2005, vol. 5808.

[5] D. E. Hack and M. A. Saville, "Analysis of SAR moving grid processing for focusing and detection of ground moving targets," in *Proc. of SPIE on Defense, Security and Sensing, Orlando, FL, USA*, April 2011, vol. 8051.

[6] S. Zhu, G. Liao, Y. Qu, Z. Zhou, and X. Liu, "Ground moving targets imaging algorithm for synthetic aperture radar," *IEEE Trans. on Geoscience and Remote Sensing*, vol. 49, pp. 462–476, January 2011.

[7] L. Wang and B. Yazıcı, "Bistatic synthetic aperture radar imaging using ultranarrow-band continuous waveforms," *Under review by IEEE Trans. on Image Processing*.

[8] C. J. Nolan and M. Cheney, "Microlocal analysis of synthetic aperture radar imaging," *The Journal of Fourier Analysis and Applications*, vol. 10, pp. 133–148, 2004.

[9] M. Martorella, F. Berizzi, and B. Haywood, "Contrast maximisation based technique for 2-d ISAR autofocusing," *IEE Proc. on Radar Sonar Navig.*, vol. 152, pp. 253–262, August 2005.